

## *Electronic Supplementary Information (ESI)*

# **Impact of the hole transport layer on the space charge distribution and hysteresis in perovskite solar cells analysed by capacitance-voltage profiling**

**E. Regalado-Pérez, Evelyn B. Díaz-Cruz, and J. Villanueva-Cab**

**Instituto de Física “Luis Rivera Terrazas”, Benemérita Universidad Autónoma de Puebla,  
Ecocampus Valsequillo, C.P. 72960, San Pedro Zacachimalpa, Puebla, México**

This supporting information presents the following contents.

a.	Materials and methods	1-4
b.	Device simulation	4-8
c.	Device performance	8-11
d.	References	11

### **a) Materials and methods**

*Materials.* All chemicals were purchased from Sigma-Aldrich, Greatcell, and Lumtec and used without further purification.

*Substrate Preparation.* F-doped SnO<sub>2</sub> substrates (FTO, TEC15) were patterned by etching with Zn powder and 1 M of HCl diluted in deionised (DI) water. The etched FTO substrates were ultrasonically cleaned for 10 min each in a neutral detergent, DI water, acetone, and finally in isopropyl alcohol. The substrates were dried under a nitrogen stream and cleaned with oxygen plasma. As ETL, compact SnO<sub>2</sub> was deposited by chemical bath deposition (CBD) following the

procedure reported elsewhere<sup>1</sup>. In brief, 500 mg urea was dissolved in 400 mL DI water, followed by the addition of 10  $\mu$ L thioglycolic acid and 0.5 mL HCl (37 wt%). Later, 0.1g  $\text{SnCl}_2 \cdot 2\text{H}_2\text{O}$  was added to this solution and stirred for 5 min. The FTO substrates were immersed in the above solution under magnetic agitation for 4 h at 80 °C, washed with DI water and dried under a nitrogen stream. Finally, the films were annealed at 200 °C for 30 min. in a muffle furnace under ambient air. The  $\text{SnO}_2$  substrates were treated with oxygen plasma for 15 min. before being transferred into the  $\text{N}_2$ -filled glove box for perovskite deposition.

*Perovskite Solar Cell Fabrication.* Devices were fabricated using mixed-cation lead mixed-halide perovskite with the nominal formula  $[\text{FAPbI}_3]_{83}[\text{MAPbBr}_3]_{17}$ . The final perovskite solution was prepared by mixing  $\text{FAPbI}_3$  (1.22 M) and  $\text{MAPbBr}_3$  (1.22 M) solutions in a DMF:DMSO solvent mixture (4:1, v/v) at a volume ratio of 83:17, according to previously reported procedure<sup>2</sup>. To prepare the  $\text{FAPbI}_3$  solution, 350 mg of FAI was dissolved in a 1.5 M  $\text{PbI}_2$  solution (1151 mg of  $\text{PbI}_2$  in 1660  $\mu$ L of DMF:DMSO). Similarly, the  $\text{MAPbBr}_3$  solution was prepared by dissolving 48 mg of MABr in a 1.5 M  $\text{PbBr}_2$  solution (187 mg of  $\text{PbBr}_2$  in 340  $\mu$ L of DMF:DMSO). The perovskite layers were deposited by a one-step spin-coating at 3500 rpm for 30 s, and 10 s before the end, 150  $\mu$ L of green antisolvent ethyl acetate (EA) was dropped onto the  $\text{SnO}_2$ /FTO substrate. After that, the sample was annealed on a hot plate at 100°C for 30 min. As HTL, a thin film of CuSCN or Spiro-OMeTAD was deposited onto the perovskite layer. For the CuSCN deposition, a solution consisting of 30 mg CuSCN in 1 mL diethyl sulphide was spin-coated at 4000 rpm for 30 s. Spiro-OMeTAD was deposited from a 70 mM solution in chlorobenzene, containing FK269 as a dopant and additives Li-TFSI and t-BP. The Spiro-MeOTAD solution was spin-coated on the perovskite layer at 3000 rpm for 30 s. Finally, the devices were completed by evaporating 80 nm Au film as the electrode with an active area of 0.1  $\text{cm}^2$ .

*Device characterisation.* Electrochemical impedance spectroscopy (EIS) measurements were performed under AM1.5 illumination using a Zennium potentiostat (Zahner Elektrik). Nyquist plots were fitted using EC Lab software. The current-voltage (J-V) characteristics were measured under AM1.5G illumination from a solar simulator Sol3A Class AAA (Oriel

Instruments). The incident light power was adjusted to 1000 W/m<sup>2</sup> using a calibrated Si reference cell supplied by Newport (91150V). Six cells, each with an active area of 0.1 cm<sup>2</sup>, were prepared on a 2.0 cm × 2.5 cm substrate using mechanical scribing. The voltage scan rate was 10 mV s<sup>-1</sup>, and no device preconditioning was applied before starting the measurement. The external quantum efficiency (**EQE**) was measured using a QEPVSI-B (Newport) system in the wavelength range of 300 to 1100 nm. The light intensity at different wavelengths was calibrated using a UV-enhanced Si photodetector (71889, Newport). The **C-V** characteristics were performed using a C-V Analyzer (4200-SCS, Keithley), measuring in two scan directions: forward bias to short-circuit and short-circuit to forward bias. The measurement frequency for C-V characteristics was 100 KHz and 10 mV AC perturbation. The cells were kept in the dark at room temperature to allow them to reach equilibrium.

*Device simulation.* The J-V and C-V characteristics of PSCs were simulated using the Drifusion code, which is based on a drift-diffusion model involving the solution of Poisson's equation together with the continuity equations for electrons, holes, and mobile ions. The mobile cation density "c" is initially balanced by a uniform static counter-ion density N<sub>cat</sub>, while the mobile anion density "a" is similarly balanced by a static ion density N<sub>ani</sub>. For the one-dimensional system under consideration, Poisson's equation can be explicitly expressed as<sup>3</sup>:

$$\frac{d^2\varphi(x,t)}{dx^2} = -\frac{q(x,t)}{\varepsilon_0\varepsilon_r(x)}[p(x,t) - n(x,t) + N_D(x) - N_A(x) + \dots \\ z_c c(x,t) + z_a a(x,t) - z_c N_{cat}(x) - z_a N_{ani}(x)], \quad (\text{S1})$$

where  $\varepsilon_0$  is the permittivity of the free space,  $q$  is the elemental charge,  $\varphi$  is the electrostatic potential, and  $p$ ,  $n$ ,  $c$ , and  $a$  are free holes, free electrons, cations, and anions, respectively.  $N_A$  refers to the ionised acceptor-like doping concentration, and  $N_D$  is the ionised donor-like doping concentration.  $N_{cat}$  and  $N_{ani}$  correspond to cation and anion concentrations, respectively.  $z_c$  and  $z_a$  are the integer charge states for the ionic species (typically  $z_c=1$ , and  $z_a=-1$ )

In one dimension, the continuity equations for electrons, holes, cations and anions are given by<sup>3</sup>

$$\frac{\partial n(x,t)}{\partial t} = -\frac{\partial J_n(x,t)}{\partial x} + g_n(x,t) - r_n(x,t) , \quad (\text{S2})$$

$$\frac{\partial p(x,t)}{\partial t} = -\frac{\partial J_p(x,t)}{\partial x} + g_p(x,t) - r_p(x,t) \quad (\text{S3})$$

$$\frac{\partial c(x,t)}{\partial t} = -\frac{\partial J_c(x,t)}{\partial x} + g_c(x,t) - r_c(x,t) \quad (\text{S4})$$

$$\frac{\partial a(x,t)}{\partial t} = -\frac{\partial J_a(x,t)}{\partial x} + g_a(x,t) - r_a(x,t) \quad (\text{S5})$$

## b) Device simulation

The device architecture of the perovskite solar cells proposed in the drift-diffusion simulation reproduces the devices fabricated. The simulations explore the HTL parameters and their impact on C-V characteristics. The main simulation parameters are summarised in Table S1. For further details, the scripts (.m) and input files (.csv) used in the device simulations are available on the Zenodo repository: <https://doi.org/10.5281/zenodo.13732608>.

**Table S1.** Principal input parameters of the device simulation.

Parameters	SnO <sub>2</sub> (ETL)	Perovskite* (Absorber)	Spiro- MeOTAD (HTL)	CuSCN (HTL)
Thickness (μm)	0.100	0.450	0.250	0.250
Bandgap (eV)	3.2	1.6	2.8	3.7
Electron affinity (eV)	-4.1	-3.8	-2.3	-1.5
CB density of states (1/cm <sup>3</sup> )	1E19	1E19	1E19	1E19
VB density of states (1/cm <sup>3</sup> )	1E19	1E19	1E19	1E19
Electron mobility (cm <sup>2</sup> /Vs)	1E-1	20	1E2	1E2
Hole mobility (cm <sup>2</sup> /Vs)	1E-1	20	1E2	1E2
Cation mobility (cm <sup>2</sup> /Vs)	0	1E-10	0	0
Anion mobility (cm <sup>2</sup> /Vs)	0	1E-10	0	0
Donor concentration (1/cm <sup>3</sup> )	3E16	3.6E5	0	0
Acceptor concentration (1/cm <sup>3</sup> )	0	3.6E5	1E18	2E17
Cation concentration (1/cm <sup>3</sup> )	0	1E16, 1E17	0	0
Anion concentration (1/cm <sup>3</sup> )	0	1E10	0	0

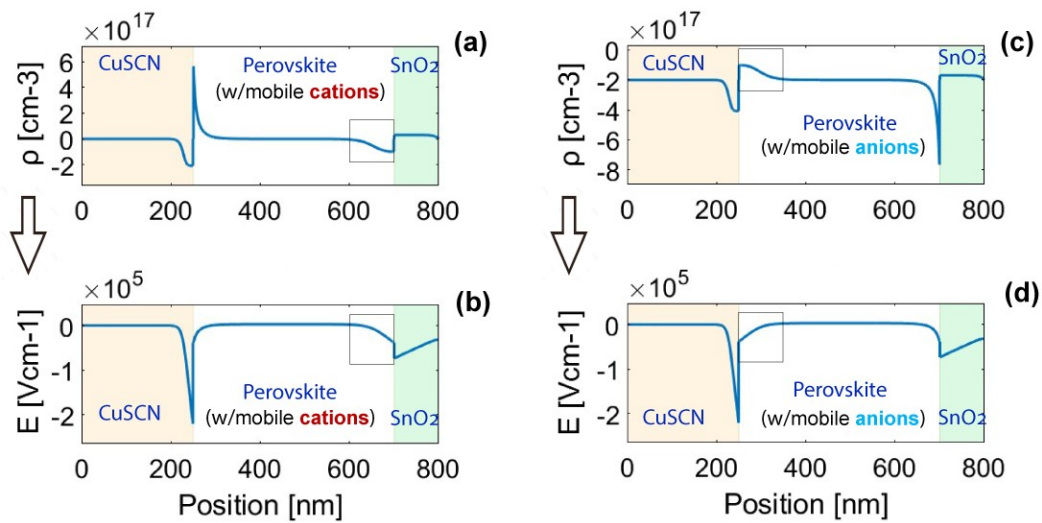


Fig. S1. Charge density ( $\rho$ ) and electric field ( $E$ ) across the perovskite device under dark and  $V=0$  for scenarios where (a), (b) cations or (c), (d) anions are the predominant mobile ions in the perovskite layer. Black rectangles at the perovskite interfaces emphasise the primary SCR.

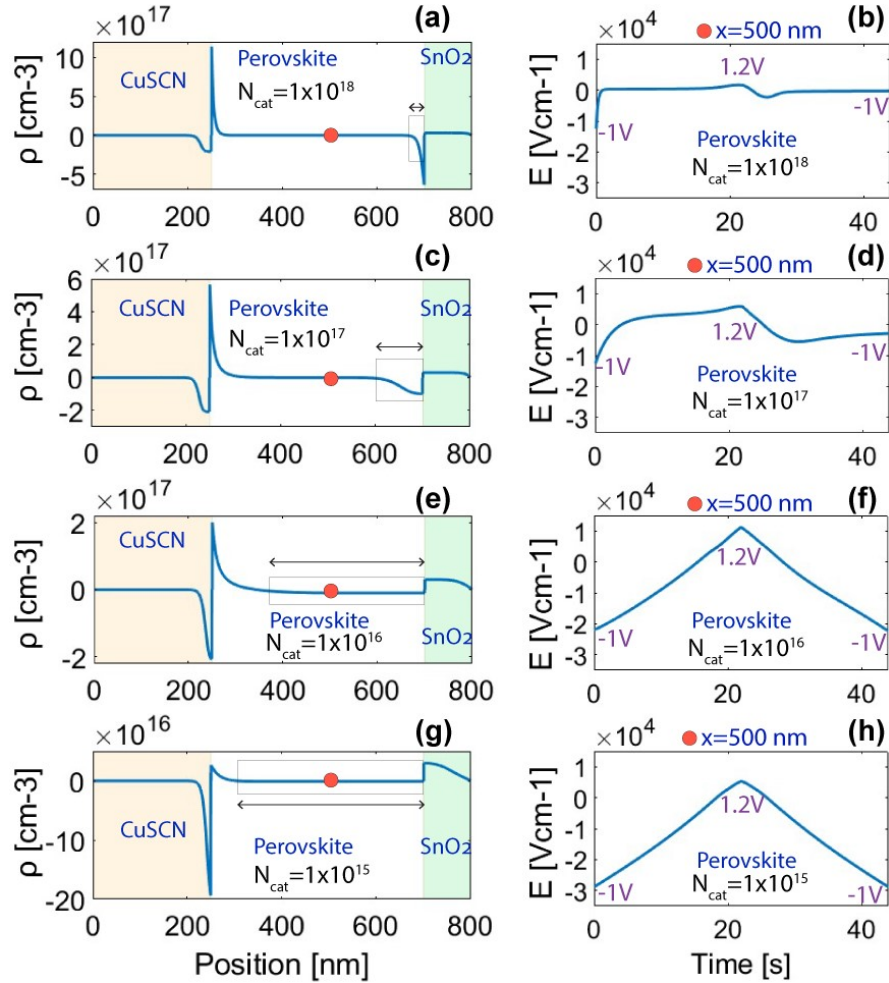


Fig. S2. (left) Electric field across perovskite device under equilibrium considering different mobile anion densities. Black rectangles on the perovskite layer illustrate how the main SCR width varies with the density of mobile cations. The red dot indicates the centre of the perovskite layer, located at  $x = 500$  nm. (right) The electric field at the centre of the perovskite layer for varying mobile cation density in the perovskite.

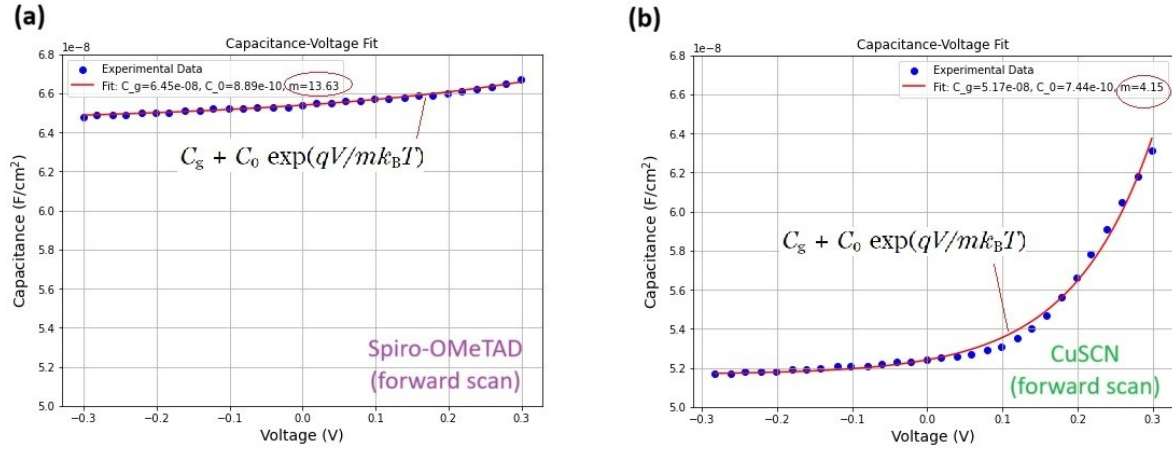


Fig. S3. C-V characteristics of perovskite solar cells with (a) Spiro-OMeTAD and (b) CuSCN as HTLs. The experimental data (blue circles) are fitted using the model  $C = C_g + C_0 \exp(qV/mk_B T)$ , where  $k_B T$  is the thermal voltage,  $C_g$  represents the geometric capacitance,  $C_0$  and  $m$  are fitting parameters that describe the slope of the C-V curve.

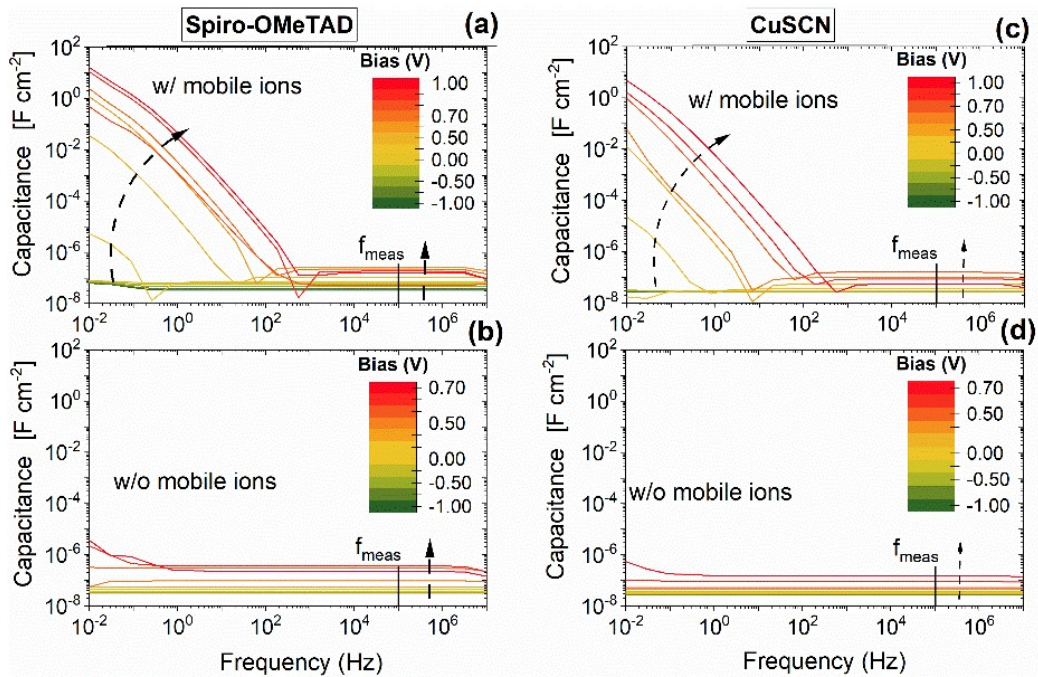


Fig. S4. Simulated capacitance-frequency (C-f) spectra for perovskite solar cells with Spiro-OMeTAD as the HTL, (a) with mobile ions and (b) without mobile ions; CuSCN as the HTL, (c) with mobile ions and (d) without mobile ions. The colour scale indicates the bias voltage. The frequency of the C-V measurements is  $f_{\text{meas}} = 100$  kHz. The arrows illustrate the increase in capacitance with bias voltage: the

curved arrow at low frequencies represents the ionic capacitance, and the vertical arrow at high frequencies indicates the geometric capacitance.

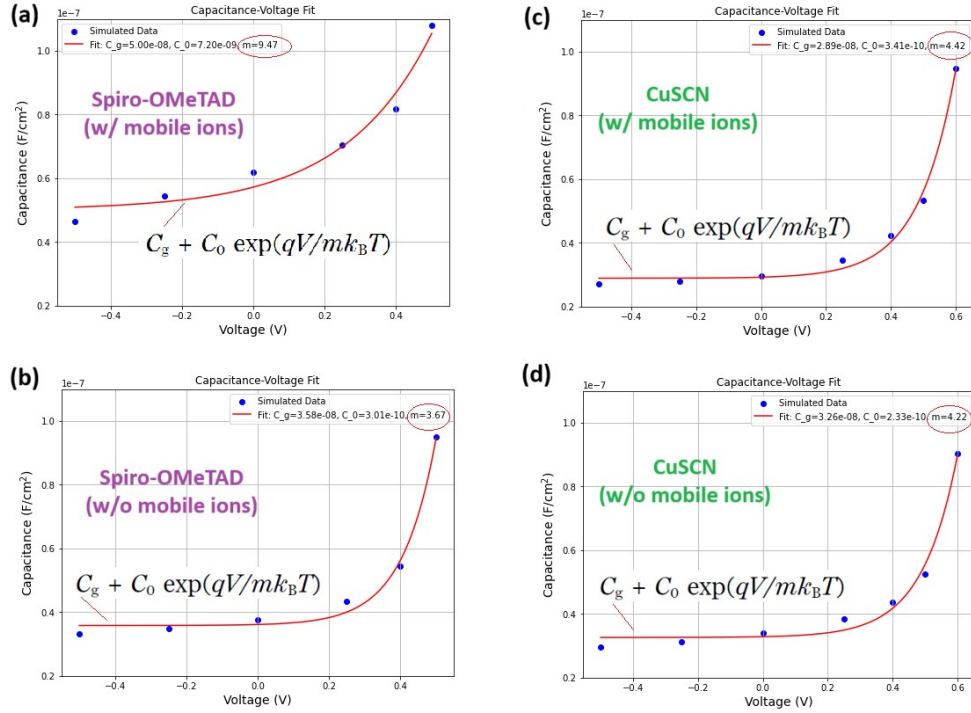


Fig. S5. Simulated C-V characteristics of perovskite solar cells with Spiro-OMeTAD and CuSCN as HTLs, with (a)&(c) and without (b)&(d) mobile ions. These data were extracted from Fig. S4 at a frequency of 100 kHz ( $f_{\text{meas}}$ ). The simulated data (blue circles) are fitted with the model  $C = C_g + C_0 \exp(qV/mk_B T)$  to extract the parameter  $m$ . Higher  $m$  values are observed for Spiro-OMeTAD devices with mobile ions, indicating slower capacitance response.

## c) Device performance

### Electrochemical Impedance Spectroscopy

We employed constant phase elements (CPE) Q2 and Q3 instead of ideal capacitors to model the non-ideal capacitive behaviour frequently observed in perovskite devices<sup>4</sup>. Although the constant phase elements reflect capacitive behaviour, an effective capacitance ( $C_{\text{eff}}$ ) is usually calculated for practical interpretation using the following equation<sup>5</sup> :

$$C_{\text{eff}} = \frac{RQ^{1/a}}{R} \quad (\text{S6})$$

where “a” is the constant phase exponent that reflects the deviation of the constant phase element from ideal capacitor behaviour. When  $a = 1$ , the CPE behaves as an ideal capacitor, where  $Q = C$ . For physically meaningful capacitance values, “a” should typically be between 0.75 and 1. While  $C_{\text{eff}}$  and the time constant ( $\tau = RC_{\text{eff}}$ ) could be determined at high frequencies, this was not possible at low frequencies for CuSCN-based devices, which exhibited an  $a_3$  value of 0.61. Parameters  $C_{\text{eff}}$  and the time constant ( $\tau$ ) for high frequencies are incorporated in Table S2. Our C-V measurements at 100 kHz correspond to this region.

**Table S2.** Equivalent circuit parameters derived from the impedance spectra in Figure 5(b).  $R_1$  is the series resistance. The resistance  $R_2$  and constant phase element  $Q_2$  represent the high-frequency component, while  $R_3$  and  $Q_3$  characterise the low-frequency component. The parameter “a” is the constant phase exponent.  $C_{\text{eff}}$  and  $\tau_2$  are the effective capacitance and time constant associated with the high-frequency component.

HTL	$R_1$ (Ohm)	$R_2$ (Ohm)	$Q_2$ $\times 10^{-9}$ ( $F s^{a-1}$ )	$a_2$	$C_{\text{eff}_2}$ $\times 10^{-9}$ (F)	$\tau_2$ $\times 10^{-6}$ (s)	$R_3$ (Ohm)	$Q_3$ $\times 10^{-4}$ ( $F s^{a-1}$ )	$a_3$
Spiro-OMeTAD	19.84	297.06	11	1	11.0	3.26	8.6E3	3.4	0.82
CuSCN	22.46	172.35	22	0.95	11.4	2.15	1.6E16	9.5	0.61

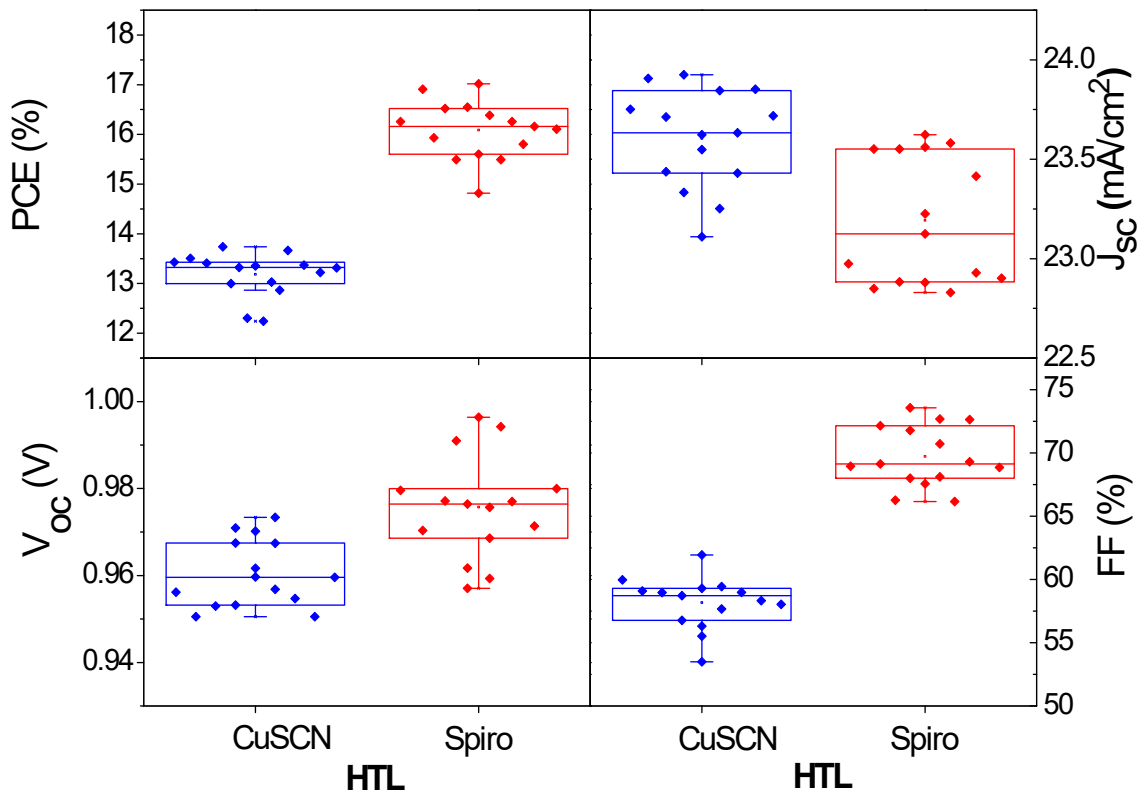


Fig. S6. Statistical values of photovoltaic parameters for the perovskite devices based on Spiro-OMeTAD or CuSCN as HTL. (15 devices were measured for each condition).

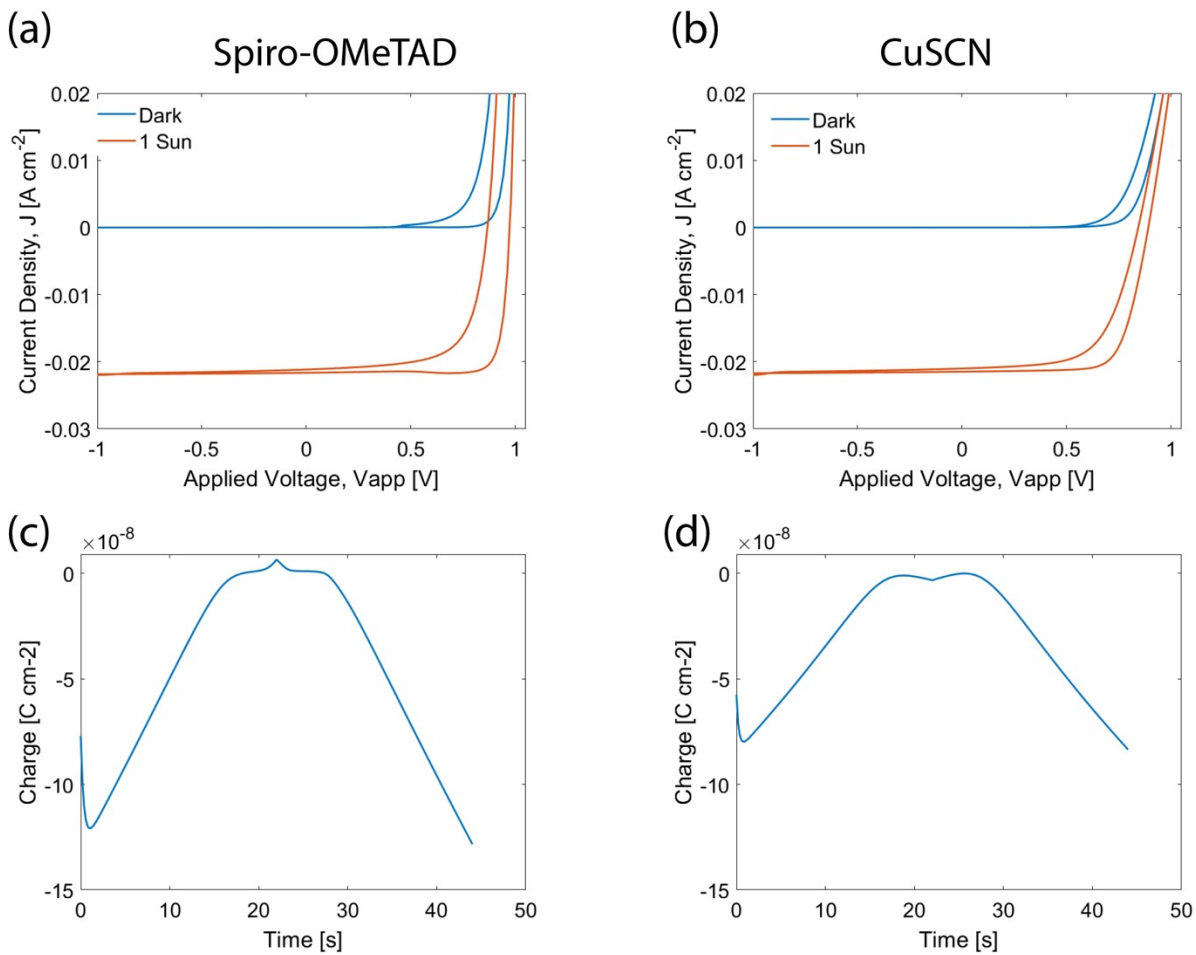


Fig. S7. (a),(b) Simulated J-V characteristics in the dark and under 1 Sun, and (c),(d) the surface charge accumulated at perovskite/HTL interface during the J-V scan. These results were obtained during a voltage scan from -1 V to 1.2 V and back, conducted at a scan rate of 100 mV/s.

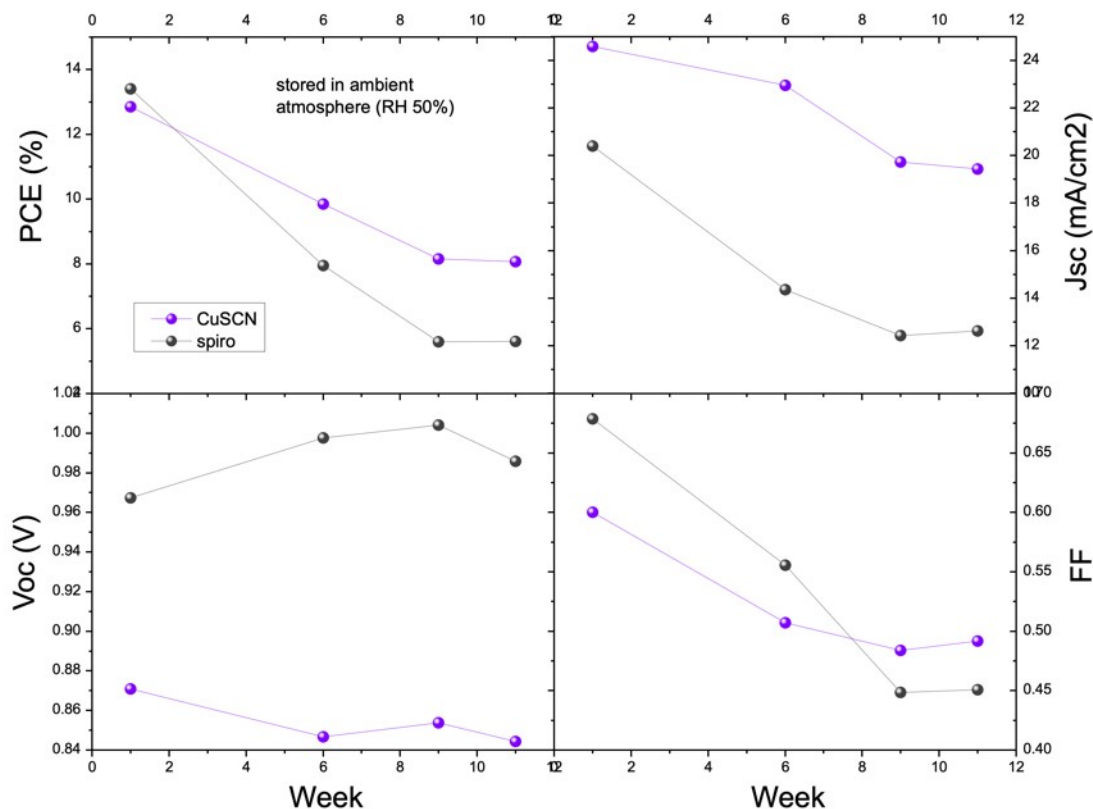


Fig. S8. Stability of photovoltaic parameters corresponding to PSCs employing different HTLs. The devices were stored for 11 weeks in ambient air with 50% relative humidity.

## d) References

- 1 E. Regalado-Pérez, E. B. Díaz-Cruz, J. Landa-Bautista, N. R. Mathews and X. Mathew, *ACS Appl. Mater. Interfaces*, 2021, **13**, 11833–11844.
- 2 M. Saliba, J.-P. Correa-Baena, C. M. Wolff, M. Stollerfoht, N. Phung, S. Albrecht, D. Neher and A. Abate, *Chem. Mater.*, 2018, **30**, 4193–4201.
- 3 P. Calado, I. Gelmetti, B. Hilton, M. Azzouzi, J. Nelson and P. R. F. Barnes, *J Comput Electron*, 2022, **21**, 960–991.
- 4 B. Roose, K. Dey, M. R. Fitzsimmons, Y.-H. Chiang, P. J. Cameron and S. D. Stranks, *ACS Energy Lett.*, 2024, **9**, 442–453.
- 5 A. Todinova, L. Contreras-Bernal, M. Salado, S. Ahmad, N. Morillo, J. Idígoras and J. A. Anta, *ChemElectroChem*, 2017, **4**, 2891–2901.